GEOPHYSICS, VOL. 67, NO. 4 (JULY-AUGUST 2002); P. 1202–1212, 12 FIGS.
10.1190/1.1500382

Migration velocity analysis from locally coherent events in 2-D laterally heterogeneous media, Part I: Theoretical aspects

Hervé Chauris*, Mark S. Noble‡, Gilles Lambaré‡, and Pascal Podvin‡

ABSTRACT

We present a new method based on migration velocity analysis (MVA) to estimate 2-D velocity models from seismic reflection data with no assumption on reflector geometry or the background velocity field. Classical approaches using picking on common image gathers (CIGs) must consider continuous events over the whole panel. This interpretive step may be difficult—particularly for applications on real data sets. We propose to overcome the limiting factor by considering locally coherent events. A locally coherent event can be defined whenever the imaged reflectivity locally shows lateral coherency at some location in the image cube.

In the prestack depth-migrated volume obtained for an a priori velocity model, locally coherent events are picked automatically, without interpretation, and are characterized by their positions and slopes (tangent to the event). Even a single locally coherent event has information on the unknown velocity model, carried by the value of the slope measured in the CIG. The velocity is estimated by minimizing these slopes.

We first introduce the cost function and explain its physical meaning. The theoretical developments lead to two equivalent expressions of the cost function: one formulated in the depth-migrated domain on locally coherent events in CIGs and the other in the time domain. We thus establish direct links between different methods devoted to velocity estimation: migration velocity analysis using locally coherent events and slope tomography.

We finally explain how to compute the gradient of the cost function using paraxial ray tracing to update the velocity model. Our method provides smooth, inverted velocity models consistent with Kirchhoff-type migration schemes and requires neither the introduction of interfaces nor the interpretation of continuous events. As for most automatic velocity analysis methods, careful preprocessing must be applied to remove coherent noise such as multiples.

INTRODUCTION

We address the problem of 2-D estimation of the background or velocity macromodel from seismic reflection data by migration velocity analysis (MVA). This approach of velocity estimation basically uses the flatness of events in common image gathers (CIGs) as a criterion for velocity quality (Al-Yahya, 1989) (Figure 1). Most approaches that do not require picking or any assumption on the velocity field require a global optimization process to minimize or maximize a cost function defined on CIGs (Stoffa, 1989; Jin and Madariaga, 1993, 1994; Jervis et al., 1996; Docherty et al., 1997; Varela et al., 1998; Jin and Beydoun, 2000). No feasible 3-D extensions exist at the moment for data sets of realistic size. Only two methods seem to converge with a local approach: migration-based traveltime inversion (Clément, 1994; Plessix, 1996) and differential semblance optimization (Symes and Carazzone, 1991; Symes, 1993, 1998; Chauris and Noble, 1998, 2001). But even in two dimensions, these approaches remain expensive and are probably not suitable for 3-D applications.

When picking is introduced in the depth-migrated domain, approaches become tractable in three dimensions. Many developments have been proposed. However, the updating formulas to invert the velocity model are generally based on at least one of the three following simplifying assumptions: laterally invariant velocity, small offset, or horizontal reflectors. The earliest MVA methods are based on all these simplifications (Al-Yahya, 1989). Many improvements have been proposed, but all require some simplifying assumptions (Deregowski, 1990; Cox and Wapenaar, 1992; Lee and Zhang, 1992; Lafond and Levander, 1993; Liu and Bleistein, 1995; Wang et al., 1995;

Manuscript received by the Editor June 12, 2000; revised manuscript received July 26, 2001.
*Formerly Ecole des Mines de Paris, Centre de Géophysique 35, rue Saint Honoré, 77305 Fontainebleau Cédex, France; presently Shell International, Volmerlaan 8, P.O. Box 60, 2280 AB Rijswijk, The Netherlands. E-mail: h.chauris@siep.shell.com.
‡Ecole des Mines de Paris, Centre de Géophysique 35, rue Saint Honoré, 77305 Fontainebleau Cédex, France. E-mail: mark.noble@geophy.ensmp.fr; gilles.lambare@geophy.ensmp.fr; pascal.podvin@geophy.ensmp.fr.

Audebert et al., 1997; Woodward et al., 1998). In most cases, picking is introduced to select the maximum of the stack power along predefined (offset, depth) curves. Only Liu's (1997) approach, valid for any 2-D velocity field, relates the perturbations of the reflector depth to the perturbations of the velocity model. In his method, the macromodel is described by velocities and interfaces.

For most approaches proposed in the literature, picking is performed only on continuous events that must be tracked continuously over a large offset range, as illustrated in Figure 2,

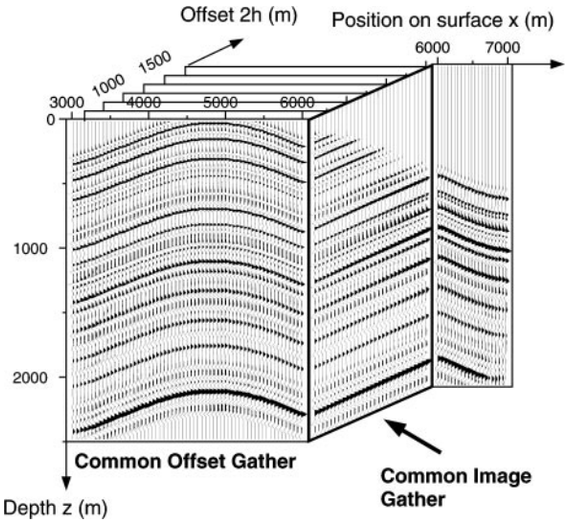

FIG. 1. Definition and use of a CIG. For 2-D data, the migrated volume is obtained by prestack depth migration of each time common-offset section with the same given velocity model. A CIG is a section in the cube, defined by a fixed position on the surface. If the exact velocity model is used for migration, then the CIG should present flat events, independent of the structure of the reflectors in the background. Events in the data are indeed replaced after migration in their exact location in the depth domain, which does not depend on acquisition parameters such as offset.

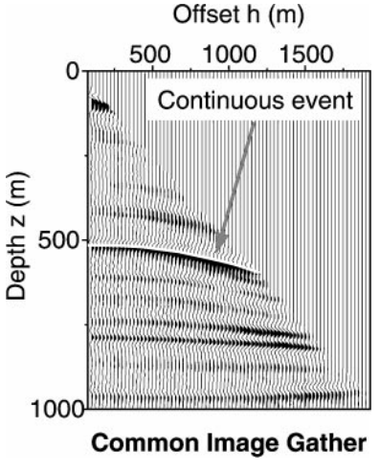

FIG. 2. Continuous event over all offsets, indicated by the white solid line. Such events are selected for inversion in the classical approaches, as in Liu (1997), where depth is picked at some sparse locations along each selected event.

and attached to a particular reflector in the model. This interpretive step is certainly the main limiting factor of present methods. It is impossible to follow continuous events in a CIG in many cases, e.g., when the tested velocity model is far from exact or in the presence of noise [see examples of a synthetic case (Figure 3) and a real case (Figure 4)].

We present a new approach valid for any 2-D velocity field and based on picking locally coherent events (Figure 5) in the depth-migrated domain. As a basic definition, a locally coherent event is defined when the reflectivity displays lateral coherency over a few neighboring traces.

Introducing locally coherent events is motivated by two reasons. From a practical point of view, it is far easier to pick many locally coherent events than to follow continuous events (Figures 3 and 4). From a theoretical point of view, velocity inversion does not require continuous events because a single locally coherent event bears information on the unknown velocity model. The initial idea is that the slope of a single locally coherent event in a CIG provides a constraint on the unknown velocity field. It should be null when the velocity field is correct.

We propose estimating the velocity field by flattening a set of locally coherent events treated as uncorrelated events (i.e., not attached to a particular reflector). Because our approach does not tie picked events to interfaces, the macromodel can be parameterized with smooth, nonblocky basis functions. A blocky parameterization could naturally be considered but is not required.

For our purpose, the main difficulty is to design a way to update the velocity model. We are thus interested in the perturbations of the depth of an event but more generally want to learn how the event is distorted (displacement and rotation) when velocity changes.

We first define a locally coherent event in a depth-migrated domain. We then explain why energy focuses in the depth-migrated domain (i.e., where it comes from) and derive a general link between the time and depth domains. These relations help specify the cost function. We finally show how to update the velocity model from the information contained in these locally coherent events using paraxial ray tracing.

Our only assumption is that the data contain only primary reflections/diffractions. In particular, we assume that careful preprocessing has removed multiples, refracted waves, and other coherent noise. This is the main limitation of the method because it is entirely automatic, including the picking step. But this difficulty is not specific to our method and is encountered by most velocity analysis processes. Apart from this assumption, we want our theory to be valid for any 2-D velocity field and an arbitrary distribution of reflectors in the subsurface, provided it is correctly sampled in the data.

DEFINING A LOCALLY COHERENT EVENT IN THE PRESTACK DEPTH-MIGRATED DOMAIN

Let us define what we call a locally coherent event in the depth-migrated volume. For a 2-D data set, migration is performed in a given velocity model, producing, in the depth domain, CIGs and common-offset gathers (COGs) (Figure 1). Local coherence is sought simultaneously around a given location (x, h) in the two sections (x, z) and (h, z) of the migrated

volume (x, z, h), where h is the half-offset. A locally coherent picked event is thus characterized by five parameters (x, z, ξ, φ, h) (Figure 5), where (x, z) is the event location in depth, ξ is its apparent geological migrated dip (as measured in the COG), and φ is its residual slope (as measured in the CIG). By definition, for each locally coherent event migrated in a given slowness 2-D model u,

$$\tan\varphi = \left.\frac{\partial z}{\partial h}\right|_{x,u}, \tag{1}$$

$$\tan\xi = \left.\frac{\partial z}{\partial x}\right|_{h,u}. \tag{2}$$

For the exact velocity model, the CIGs should present flat events (Al-Yahya, 1989). Mathematically, φ should be zero after convergence so that we use a least-squares misfit function of the form

$$J[u] = \frac{1}{2}\sum_{picks}(w\tan\varphi)^2, \tag{3}$$

where w is a weighting coefficient still to be defined. After convergence, (x, z) represents the actual location of the reflection/diffraction point in depth and ξ is the real geologic dip of the corresponding reflector. Angle φ is basically needed to determine the cost function, whereas ξ is needed to compute its gradient, as explained below.

We want to give evidence that the definition of our cost function has potentially good properties in terms of process optimization. Through the generic cost function [equation (3)], our method can be directly related with differential semblance optimization (DSO) (Symes and Carazzone, 1991; Symes, 1993, 1998; Chauris and Noble, 1998; Chauris and Noble, 2001). The associated differential semblance function J_{DS} also quantifies the flatness of seismic events in CIGs and is based on horizontal derivatives of these panels, i.e.,

$$J_{DS}[u] = \frac{1}{2}\sum_{selected\ x}\iint dz\,dh\left[\frac{\partial R}{\partial h}(x, z, h, u)\right]^2, \tag{4}$$

where $R(x, z, h, u)$ is the value (amplitude) of the prestack depth-migrated image at point (x, z, h) migrated with the slowness model u (Figure 1).

Let us consider a zoom on a migrated CIG (as in Figure 6b) with small dimensions but containing a nonzero reflectivity. The amplitude of the central trace h_0 inside the rectangle may be written as $A\omega[k(z - z_0)]$, where ω is a wavelet displayed around depth z_0, A is the amplitude of the reflectivity, and k is a stretching factor. Because we assume that the box is small enough, the other traces can be deduced from the central trace by translation as follows:

$$R(x, z, h, u) \sim A\omega[k(z - z_0 + p\cdot(h - h_0))], \tag{5}$$

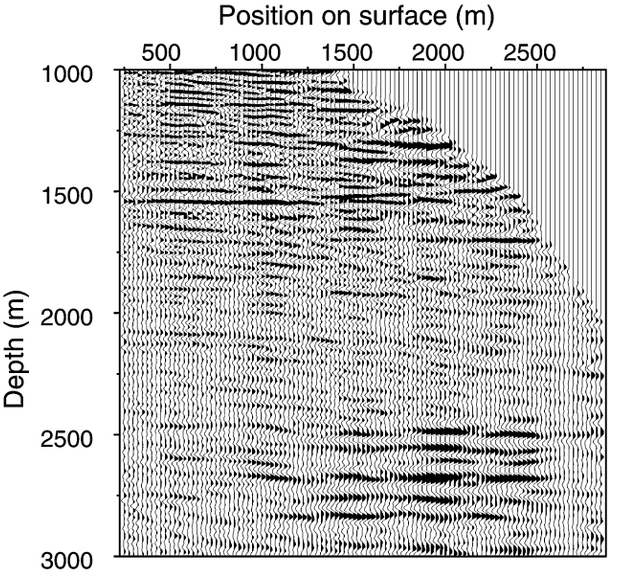

FIG. 4. CIG obtained on a real data set. It is clearly easier to pick many events with local coherency (for example, around depths 2100 or 2500 m) than to follow continuous events over all offsets, as needed in many approaches.

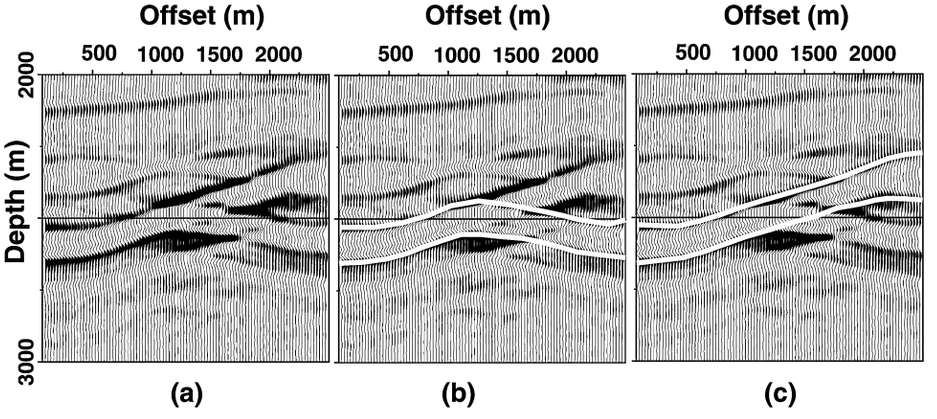

FIG. 3. (a) Even on synthetic data, it is not always easy to follow continuous events over all offsets in a CIG. (b, c) Two interpretations are proposed, indicated by the white solid curve. This effect appears, for example, when the migration velocity is not correct, even when the data only contain primary reflections/diffractions (this case) because they were generated by ray + Born approximation (Lambaré et al., 1996).

where $p = \tan\varphi$ is the slope defining how the depth of the locally coherent event changes with offset. The derivative with respect to the offset gives

$$\left.\frac{\partial R(x,z,h,u)}{\partial h}\right|_{x,z,u} \sim p \cdot kA\omega'[k(z - z_0 + p \cdot (h - h_0))]. \quad (6)$$

From that expression, it becomes clear that minimizing J_{DS} is equivalent to minimizing the residual slope $p = \tan\varphi$ in the CIG as in equation (3).

Symes (1999) demonstrates in the 1-D case that the J_{DS} cost function has a unique minimum. Thus, a gradient-type algorithm may be applied to converge to the (unique) solution. This property has not yet been proven in two (or three) dimensions. However, successful applications of DSO in two dimensions with synthetic and real data sets (Chauris and Noble, 2001) give practical evidence that the J_{DS} cost function remains well behaved.

Because of the formal analogy between J_{DS} and our generic cost function, we consider a reasonable conjecture that our problem can converge with a gradient-type optimization process.

In the following section, we demonstrate that, by establishing a link between locally coherent events in depth and time, we can choose the weighting function w in equation (3) such that the gradient of the cost function can be explicitly computed with the help of paraxial ray tracing done in the tested velocity model, whatever its complexity.

COST FUNCTION

This section is devoted to the appropriate development of the expression of the cost function. We need to understand why energy focuses in the depth-migrated domain. For this purpose, we derive the relationship between the two picked angles in the depth domain and the slopes in the time data (traveltime derivatives in the seismograms). For simplicity and clarity, all calculations are developed in the common-shot domain and are then extended to the common-offset case, which generally is preferred for applications. Because mathematical computations are rather involved, we only mention the crucial points and the final results and try to provide a physical understanding of the different steps. More details are presented in Appendix A. To derive these calculations, we must understand which parameters must be kept fixed and which can be variable.

Focusing energy in the depth-migrated domain (common-shot case)

To better understand the information contained in the residual slope $\tan\varphi$ measured in the CIG (Figure 5), we have to know why energy focuses at a certain position (x, z, h) in the depth-migrated domain. For that purpose, we need to establish the relationship between the time and depth domains in a general 2-D case (Figure 6).

To introduce the formalism we need to derive these relations, we temporarily switch to another domain. The energy focused in the image cube results from focusing the seismic events recorded in the data cube (seismograms) (s, r, t^*), where s and r denote shot and receiver positions and t^* is the recording time.

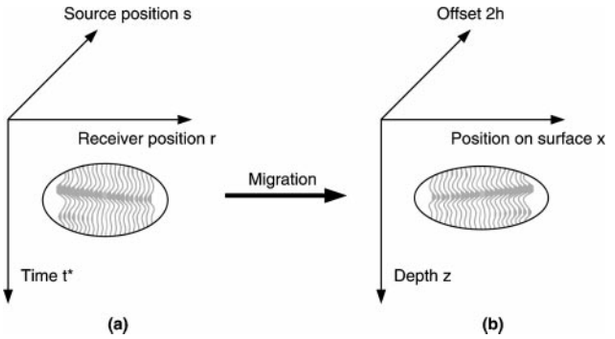

FIG. 6. Definition of (a) time and (b) depth-migrated domains. The aim is (1) to understand why a locally coherent event focuses in the depth domain and then (2) to minimize the residual slope in the CIG.

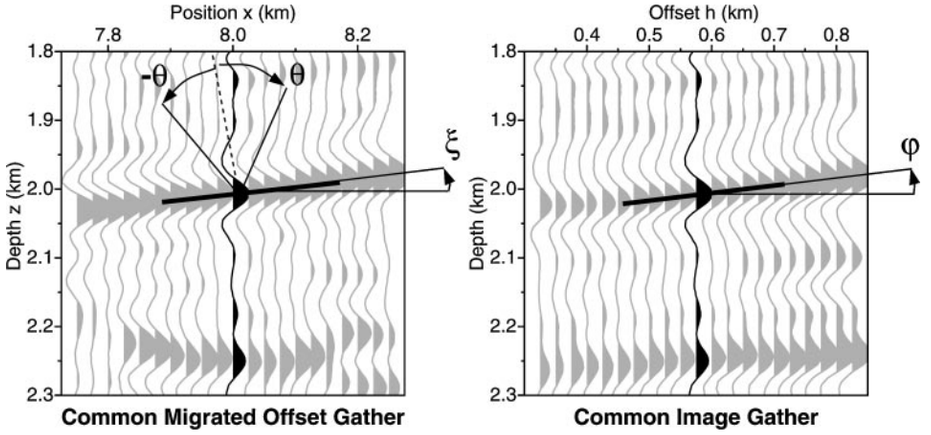

FIG. 5. The five values characterizing a locally coherent event in the 2-D prestack depth-migrated domain (x, z, ξ, φ, h). Migration at common offset is performed to obtain the COG (left) and CIG (right), where picking is performed simultaneously around the same location (x, h). The half-aperture angle θ is defined such that the two rays reach the given offset $2h$ on the surface, starting symmetrically around the normal of the dip.

In this cube, it is possible to define, by analogy, locally coherent events in time. Such an event is a wave packet displaying local coherency near the location (s, r, t^*) in the cube. Once more, defining the local coherency amounts to measuring slopes—for example, the derivatives

$$p_s^* = \left.\frac{\partial t^*}{\partial s}\right|_r, \tag{7}$$

$$p_r^* = \left.\frac{\partial t^*}{\partial r}\right|_s \tag{8}$$

of the event traveltime with respect to shot and receiver locations (Figure 7). This event is described by five parameters $(s, r, t^*, p_s^*, p_r^*)$, analogous to (x, h, z, φ, ξ). Parameters describing the event in time are objective, i.e., experimental. On the contrary, (x, h, z, φ, ξ) describing the counterpart in the image cube depend on the velocity model used for migration. In the following equations, we emphasize objective parameters with a star (e.g., p_s^*).

Image focusing is best understood in the framework of Kirchhoff migration (Schneider, 1978; Bleistein et al., 1987; Audebert et al., 1997). We first cover the case of common-shot migration. Consider a locally coherent event picked in the common-shot gather for source location s. In Figure 7, the event is characterized by the parameters (r, t^*, p_r^*). The parameter p_s^* is not accessible; it can only be measured using several shot gathers simultaneously. In common-shot migration, this event focuses somewhere along the diffraction curve, namely, the isochron (Figure 8a), implicitly defined by

$$t_s(s, x, z, u) + t_r(x, z, r, u) = t^*(s, r), \tag{9}$$

where t_s and t_r are (model-dependent) one-way traveltimes from s and r to the image point (x, z). Energy builds up constructively at one location, provided it also belongs to the envelope of the isochron (i.e., its derivative with respect to receiver position). The two focusing equations for the selected event (r, t^*, p_r^*) thus read

$$t_s(s, x, z, u) + t_r(x, z, r, u) = t^*(s, r), \tag{10}$$

$$\left.\frac{\partial t_r}{\partial r}\right|_{x,z,u} = \left.\frac{\partial t^*}{\partial r}\right|_s = p_r^*. \tag{11}$$

We now must understand what $(\partial t_r/\partial r)|_{x,z,u}$ stands for in terms of modeling. At location (x, z) on the isochron, consider the ray shot toward the receiver in the velocity model used for migration (Figure 8b). This ray reaches the surface at location r and at time t_r by construction. The second focusing equation (11) states that the event in time will focus in depth at location (x, z) such that the ray emerges at the surface with a slowness vector $\mathbf{p}_r = \nabla t$ whose horizontal component p_{rx} exactly matches the slopes p_r^* of the event in the data (Figure 8b), i.e.,

$$p_{rx} = p_r^*. \tag{12}$$

In this construction, the second slope p_s^* of the event in the data cube has not been considered. Conversely, the migrated event location and dip (x, z, ξ) are fixed by the focusing equations, but $\tan\varphi$ in the CIG remains underdetermined (because we only migrated one shot gather).

Since angle φ is measured in a CIG (i.e., at constant x), we must understand how the focusing equations change for

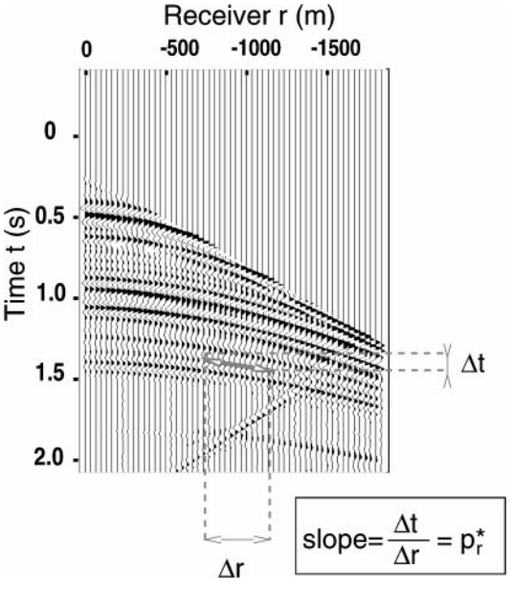

FIG. 7. Locally coherent event in the time domain. In the data, the slope is the tangent of a locally coherent reflector, measured here in a (time) common-shot gather, thus providing a slope at the receiver position.

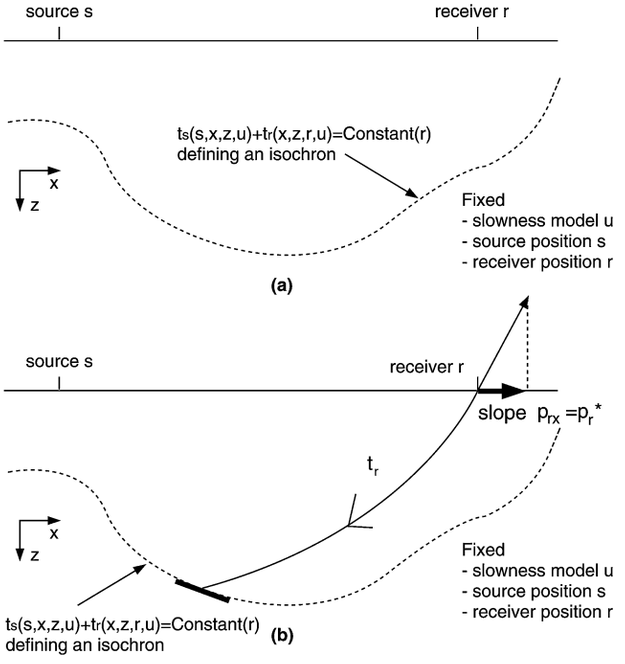

FIG. 8. Focusing a locally coherent event in the depth-migrated domain. (a) The isochron is defined in the depth domain by a constant two-way traveltime for fixed velocity-model, source, and receiver positions. (b) For migration at a constant source position, the ray is entirely defined by the position of the receiver and the slope on the surface. This horizontal component of the slowness vector corresponds to the slope in the time data (see text for explanations) as defined in Figure 7. The locally coherent event in the time domain focuses in the depth domain at the intersection of the isochron and the ray.

different s values at constant x position and constant velocity model u. All other parameters (z, s, r) in the focusing equations must be allowed to vary in the general case. Remember that $p_{rx} = p_{rx}(x, z, r, u)$ and $p_r^* = p_r^*(s, r)$. By differentiating the focusing equations (10) and (12), we obtain the following system:

$$\left(\left.\frac{\partial t_s}{\partial z}\right|_{s,x,u} + \left.\frac{\partial t_r}{\partial z}\right|_{x,r,u}\right)\delta z + \left.\frac{\partial t_s}{\partial s}\right|_{x,z,u}\delta s + \left.\frac{\partial t_r}{\partial r}\right|_{x,z,u}\delta r = p_s^*\delta s + p_r^*\delta r, \tag{13}$$

$$\left.\frac{\partial p_{rx}}{\partial z}\right|_{r,x,u}\delta z + 0\cdot\delta s + \left.\frac{\partial p_{rx}}{\partial r}\right|_{x,z,u}\delta r = \left.\frac{\partial p_r^*}{\partial s}\right|_{r}\delta s + \left.\frac{\partial p_r^*}{\partial r}\right|_{s}\delta r. \tag{14}$$

Using equation (11), the last term on the left side of equation (13) is balanced by the second term on the right side, providing a new system of linear equations:

$$\left(\left.\frac{\partial t_s}{\partial z}\right|_{s,x,u} + \left.\frac{\partial t_r}{\partial z}\right|_{r,x,u}\right)\delta z + p_{sx}\delta s = p_s^*\delta s, \tag{15}$$

$$\left.\frac{\partial p_{rx}}{\partial z}\right|_{r,x,u}\delta z + \left.\frac{\partial p_{rx}}{\partial r}\right|_{x,z,u}\delta r = \left.\frac{\partial p_r^*}{\partial s}\right|_{r}\delta s + \left.\frac{\partial p_r^*}{\partial r}\right|_{s}\delta r, \tag{16}$$

where

$$\left.\frac{\partial p_r^*}{\partial s}\right|_{r} = \left.\frac{\partial^2 t^*}{\partial s^2}\right|_{r} \quad \text{and} \quad \left.\frac{\partial p_r^*}{\partial r}\right|_{s} = \left.\frac{\partial^2 t^*}{\partial r^2}\right|_{s}$$

are directly linked to the curvature of the locally coherent event in the time domain. Fortunately, they do not appear in the expression needed for $z(s)$ that we are interested in. Indeed, the definition from equation (1) leads to

$$\tan\varphi = \left.\frac{\partial z}{\partial s}\right|_{x,u} = \frac{p_s^* - p_{sx}}{\left.\frac{\partial t_s}{\partial z}\right|_{s,x,u} + \left.\frac{\partial t_r}{\partial z}\right|_{r,x,u}}. \tag{17}$$

The denominator is computed in Appendix A, and we finally obtain

$$\tan\varphi = \frac{p_s^* - p_{sx}}{2u\cos\theta\cos\xi}, \tag{18}$$

where u is the value of the slowness at the scattering point (x, z). We define $\alpha = 2u\cos\theta\cos\xi$. This term equals zero for vertical dips and direct (transmitted) arrivals that are generally not taken into account during migration. It is related to the stretching factor occurring in migration (Tygel et al., 1994).

To summarize, we obtain two equations valid for any 2-D velocity field and any reflector geometry:

$$p_r^* - p_{rx} = 0, \tag{19}$$

$$p_s^* - p_{sx} = \alpha\tan\varphi. \tag{20}$$

Thus, $p_s^* = p_{sx}$ for the exact velocity field (i.e., $\tan\varphi = 0$). Velocity estimation is equivalent to adjusting the horizontal slowness provided by ray tracing to the actual slopes of the seismic event in the (time) data space. This important point is discussed further below. In spite of their very simple form, equations (19) and (20) have been established for the general case. In particular, no hypothesis on the curvature of the event is necessary.

Common-offset case

The approach is very similar to the common-shot case. We define the half-offset $h = (s - r)/2$ and the midpoint $m = (s + r)/2$. For simplicity, we introduce the slope components in the relevant (h, m) domain,

$$p_{hx} = \frac{p_{sx} - p_{rx}}{2}, \tag{21}$$

$$p_{mx} = \frac{p_{sx} + p_{rx}}{2}, \tag{22}$$

and the equivalent equations for the slopes measured in the time data,

$$p_h^* = \frac{p_s^* - p_r^*}{2}, \tag{23}$$

$$p_m^* = \frac{p_s^* + p_r^*}{2}. \tag{24}$$

During the migration and for each offset the summation is performed over all midpoints m. By replacing the roles of s and r by the variables h and m, we obtain equations similar to the common-shot case:

$$t_s(s, x, z, u) + t_r(x, z, r, u) = t^*(h, m), \tag{25}$$

$$\left.\frac{\partial(t_s + t_r)}{\partial m}\right|_{x,z,h,u} = \left.\frac{\partial t^*}{\partial m}\right|_{h}. \tag{26}$$

Equations (25) and (26) indicate where energy focuses in the depth-migrated domain. To obtain the relation equivalent to equation (18), we must differentiate equations (25) and (26) with respect to z, h, and m for constant x and u. Using exactly the same approach as developed for the common-shot case, we finally obtain

$$p_m^* - p_{mx} = 0, \tag{27}$$

$$p_h^* - p_{hx} = \frac{\alpha}{2}\tan\varphi, \tag{28}$$

or, equivalently,

$$(p_s^* - p_{sx}) + (p_r^* - p_{rx}) = 0, \tag{29}$$

$$(p_s^* - p_{sx}) - (p_r^* - p_{rx}) = \alpha\tan\varphi. \tag{30}$$

Focusing relation (29) states that the sum of the two horizontal slowness components (at source and receiver) is constant and independent of the velocity model used for migration. Conversely, the difference between the slopes is directly related to the slope measured in the CIG [equation (30)].

Cost functions

To more easily compute the gradient of the cost function, we introduce $w = \alpha = 2u\cos\theta\cos\xi$ as the weighting term to apply in equation (3). Our cost function thus reads in the common-shot case

$$J[u] = \frac{1}{2}\sum_{picks}[\alpha\tan\varphi]^2 \tag{31}$$

$$= \frac{1}{2}\sum_{picks}(p_{sx} - p_s^*)^2. \tag{32}$$

To calculate the cost function in a given velocity model, let's use the picked data in the migrated domain and relation (31). Equation (32) is only used to compute the gradient of the cost function because p_s^* does not depend on the velocity chosen for migration.

The common-offset case is very similar to shot profile migration. Once again, a convenient cost function can be designed from relation (28):

$$J[u] = \frac{1}{2}\sum_{picks}[\alpha \tan\varphi]^2 \tag{33}$$

$$= 2\sum_{picks}(p_h^* - p_{hx})^2 = 2\sum_{picks}(p_{sx} - p_s^*)^2$$

$$= 2\sum_{picks}(p_{rx} - p_r^*)^2, \tag{34}$$

where the formulations in equation (34) are obtained using equations (29) and (30).

Whatever the migration scheme (common shot or common offset), the criterion compares computed slopes and observed slopes, although no slope is picked in the time data. We now illustrate this point in the following section.

Time versus depth domain for velocity estimation

Different but equivalent expressions have been obtained for the cost function for both the common-shot case with equations (31) and (32) and the common-offset case with equations (33) and (34). Minimizing residual slopes in the CIGs or fitting computed slopes to observed slopes in the time data is equivalent. These relations establish direct links between different methods devoted to velocity estimation, namely, our method, working in the depth-migrated domain on locally coherent events (Stork, 1992; Wang et al., 1995; Woodward et al., 1998), and slope tomography methods, also using locally coherent events but in the time domain (Sword, 1987; Biondi, 1992; Billette and Lambaré, 1998).

With slope tomography methods, velocity is estimated from traveltimes and slopes picked in the time domain on locally coherent events. With stereotomography, a general slope tomography method (Billette and Lambaré, 1998), the model is described by the velocity model itself and scattering points. These points are characterized by their position, dip, and corresponding aperture angles (Figure 9). For each picked event, data (two-way traveltime, positions, and slopes at the source and receiver) are calculated by shooting rays from the scattering point to the surface. The associated cost function is the difference between observed and calculated data. It can be expressed as a weighted summation:

$$J_{stereo}[u] = \frac{1}{2}\sum_{picks}\big[w_{s_x}(s_x - s^*)^2 + w_{s_z}(s_z - 0)^2$$
$$+ w_{r_x}(r_x - r^*)^2 + w_{r_z}(r_z - 0)^2$$
$$+ w_{ps}(p_{sx} - p_s^*)^2 + w_{pr}(p_{rx} - p_r^*)^2$$
$$+ w_t(t_s + t_r - t^*)^2\big]. \tag{35}$$

The inversion consists of simultaneously retrieving the ray segments $(x, z, \theta, \xi, t_s, t_r)$ and the slowness model u. In MVA, the positions are obtained automatically by migration (even for a wrong velocity model). Thus, the total traveltime and the positions of the source and receiver associated with a ray segment match by construction. For common-shot migration, we established in equation (12) that $p_{rx} = p_r^*$. The cost function thus becomes

$$J_{stereo}[u] = \frac{1}{2}\sum_{picks} w_{ps}(p_{sx} - p_s^*)^2, \tag{36}$$

as proposed in equation (32).

These relations let us unify totally different approaches for velocity estimation: MVA in the depth domain and slope tomography in the time domain. However, their implementations are rather different. For example, the coverage of the picked events in the depth domain is more uniform for the MVA method; picking should be easier because it is done in the migrated domain. Since we have defined in detail the cost function that we adopt here and have shown the physical meaning of the residual slope in the CIG, we can now explain how to update the velocity model.

COST FUNCTION GRADIENT

An easy way to obtain the gradient of the cost function could be to compute it by finite differences, requiring at least as many migrations as the number of parameters describing the velocity model. However, this solution is in efficient. We therefore develop an explicit formulation of the expression of the gradient valid for any 2-D velocity fields. Like the cost function, we first present the common-shot case.

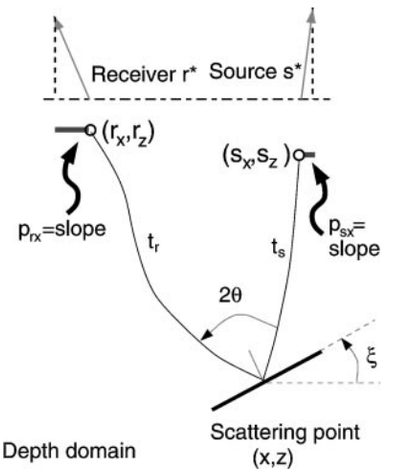

FIG. 9. In stereotomography (Billette and Lambaré, 1998), a general slope tomography method, the observed data consist of $(s^*, r^*, t^*, p_s^*, p_r^*)$, picked on seismograms. The model is given by the velocity model itself and the positions of the scattering points, defined by $(x, z, t_s, t_r, \theta, \xi)$. The cost function compares the characterized values at the extremities of the two ray segments from the scattering points to the data. In our method, the positions of the ray segment are automatically retrieved by migration, i.e., $s_x = s^*$, $s_z = 0$, $r_x = r^*$, $r_z = 0$, $t_s + t_r = t^*$. For migration at a common source, we also have $p_{rx} = p_r^*$. Only the slope at the source position may differ from the observed slope, providing a simpler cost function given by equation (36).

Common-shot case

The computation is performed for a given velocity model, which can be far from the exact velocity field. We have to understand how to relate the perturbations of the positions (x, z) and angles (ξ, θ, φ) to perturbations of the velocity model. Since p_s^* is independent of the tested velocity field, the gradient of the cost function can be formulated as

$$\frac{\partial J[u]}{\partial u} = \sum_{picks}(p_{sx} - p_s^*)\frac{\partial p_{sx}}{\partial u}\bigg|_{s,r,t,p_{rx}} \tag{37}$$

$$= -\sum_{picks}\alpha \tan\varphi \frac{\partial p_{sx}}{\partial u}\bigg|_{s,r,t,p_{rx}}. \tag{38}$$

Equation (38) is obtained using equation (20). In a given velocity model, we have to understand how an elementary part of the image—namely, a locally coherent event in the depth domain—is distorted when a perturbation of the slowness field is added to the model (Figure 10). All variables in the depth domain—position x, depth z, and scattering angles $\theta_s = \xi + \theta$ and $\theta_r = \xi - \theta$—depend on the tested velocity model. The perturbations δx, δz, $\delta\theta_s$, and $\delta\theta_r$ are constrained by two conditions at the surface, which are illustrated in Figure 10:

1) The locally coherent event is the same in the time domain, meaning that the rays shot toward the surface reach exactly the same source and the same receiver with the same double traveltime: $ds = 0$, $dr = 0$, and $dt = d(t_s + t_r) = 0$.
2) The ray toward the receiver reaches the surface with exactly the same horizontal slowness vector: $dp_{rx} = 0$ [focusing condition (12)]. Indeed, p_s^* does not depend on the velocity model chosen for migration and thus p_{rx} is constant.

In a given velocity model, the perturbations of the final conditions ds, dr, dp_{sx}, dp_{rx}, and dt can be expressed using the paraxial ray theory (Farra and Madariaga, 1987) from the perturbations of initial conditions δx, δz, $\delta\theta_s$, and $\delta\theta_r$ and the slowness field δu as explained in Appendix B. Solving this linear system, we finally obtain for the Fréchet derivatives

$$\frac{\partial p_{sx}}{\partial u}\bigg|_{s,r,t,p_{rx}} = \frac{\det\left|\dfrac{\partial(p_{sx}, s, r, t, p_{rx})}{\partial(u, x, z, \theta_s, \theta_r)}\right|}{\det\left|\dfrac{\partial(s, r, t, p_{rx})}{\partial(x, z, \theta_s, \theta_r)}\bigg|_u\right|}. \tag{39}$$

Conditions where the gradient of the cost function becomes infinite are discussed later.

Common-offset case

Analogous to the development of the cost function, the common-offset case is very similar to the common-shot approach. The gradient of the cost function with respect to velocity can be expressed as

$$\frac{\partial J[u]}{\partial u} = -\frac{1}{2}\sum_{picks}\alpha \tan\varphi \frac{\partial p_{hx}}{\partial u}\bigg|_{h,m,t,p_{mx}}. \tag{40}$$

The gradient is obtained as before with two conditions, giving $\delta\theta_s$, $\delta\theta_r$, δx, and δz (Figure 11):

1) The locally coherent event is the same in the time domain, meaning that the rays toward the surface reach exactly the same offset and the same midpoint with the same double traveltime: $dh = 0$, $dm = 0$, and $dt = 0$ (or, equivalently, $ds = 0$, $dr = 0$, and $dt = 0$).
2) The summation of the horizontal slowness vectors at the surface is constant: $dp_{sx} + dp_{rx} = 2dp_{mx} = 0$ [focusing condition (27)].

The first two conditions are the same as in the common-shot case (same locally coherent event in the time data).

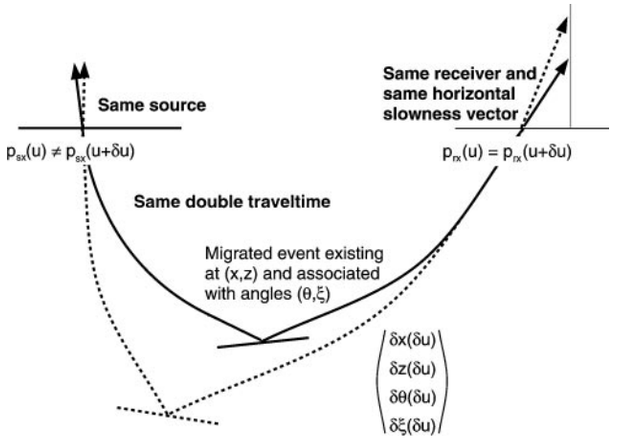

FIG. 10. Position of the migrated locally coherent events in two slightly different velocity models in a common-shot migration. All variables defined in depth (x, z, ξ, and θ) change. Their perturbations δx, δz, $\delta\xi$, and $\delta\theta$ are constrained by (1) constant position of the source and the receiver, constant double traveltime (fixed locally coherent event in the time domain), and (2) constant slope at the receiver position at the surface (common shot migration scheme). See text for more details.

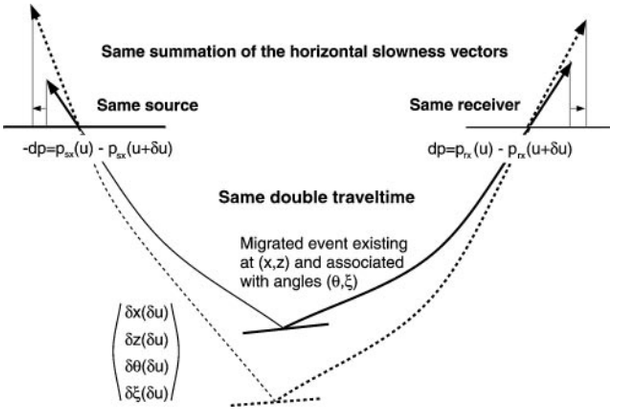

FIG. 11. Position of the migrated locally coherent events in two slightly different velocity models in a common-offset migration. The perturbations δx, δz, $\delta\xi$, and $\delta\theta$ must be evaluated to estimate the gradient of the cost function. They are constrained by (1) fixed position of the source and the receiver, constant double traveltime (same locally coherent event in the time domain), and (2) constant summation of the slopes at the source and receiver positions at the surface (common-offset migration scheme). More details are provided in the text.

We finally obtain, after computations (see Appendix B for details),

$$\left.\frac{\partial p_{hx}}{\partial u}\right|_{h,m,t,p_{mx}} = \frac{\det\left|\dfrac{\partial(p_{hx},h,m,t,p_{mx})}{\partial(u,x,z,\xi,\theta)}\right|}{\det\left|\left.\dfrac{\partial(h,m,t,p_{mx})}{\partial(x,z,\xi,\theta)}\right|_u\right|}. \qquad (41)$$

The expression of the gradient of the cost function is a combination of first-order paraxial quantities, which can be calculated using the classical ray theory (Farra and Madariaga, 1987).

Imaging condition

The final expression of the gradient of the cost function is given by equation (39) for migration at a common source. Here we examine the validity of this expression; in other words, in which cases the denominator is not equal to 0:

$$\det\left|\left.\frac{\partial(s,r,t,p_{rx})}{\partial(x,z,\theta_s,\theta_r)}\right|_u\right| \neq 0. \qquad (42)$$

An equation similar to equation (42) has been interpreted by Xu et al. (1999) as an imaging condition required to compute and use CIGs. Indeed, common-shot migration is not always possible for complex velocity fields with caustics (Nolan and Symes, 1996; ten Kroode and Smit, 1997; Xu et al., 1999). Spurious effects may be observed, such as nonflat events in CIGs when the exact velocity field has been used for migration (Nolan and Symes, 1996; Xu et al., 2001). The approach developed by Xu et al. (1999) may be extended easily to a wrong migration velocity model, leading to the same conclusion: A CIG is artifact free when relation (42) is verified. This property is known as the imaging condition.

In conclusion, we encounter the same theoretical difficulties to obtain an artifact-free CIG or to compute the gradient of the cost function. We may encounter some difficulties in very complicated velocity models with triplicated rayfields. In this case, other migration schemes must be considered, such as common angle migration (Xu et al., 1999).

THE OPTIMIZATION SEQUENCE

Now we move from theoretical aspects to a more practical point of view. The velocity is estimated from the picked events by looping over the following steps.

First, we prestack depth migrate the 2-D data set to compute some selected CIGs and COGs (Figure 1). The velocity model used for migration is the tested velocity field.

Second, we pick locally coherent events [i.e., $\xi(x,z,u)$ and $\varphi(x,z,u)$] in the computed CIGs and COGs. If $\varphi \neq 0$ for all picked events, the velocity model used for migration should be updated. For a given migrated trace, picking is performed by computing local slant stacks (Schultz and Claerbout, 1978). The slant stack, weighted by a Hamming window centered on the trace, measures at every depth the local coherence simultaneously in the two panels: CIG and COG (Figure 5). Picking automatically selects depths and associated angles where the local coherency is maximum. An equivalent tool for the time domain has been developed by Billette et al. (1998) and automated. Working in the depth-migrated domain has the advantage that the S/N ratio is generally higher than in the time data, even after migration with a wrong velocity model (Adler, 1996).

Finally, we ray trace from all picked events up to the surface to compute the gradient of the cost function and to update the velocity field. This step involves searching for two specular rays starting symmetrically with respect to the normal to the dip defined by ξ and reaching the surface with the offset associated to the picked event. As directly adapted, paraxial ray theory (Červený et al., 1977; Farra and Madariaga, 1987) is used to compute the needed expressions—in particular, the Fréchet derivatives [equation (41)].

Refer to Chauris et al. (2002) for applications on 2-D synthetic and real data sets, including more details on practical aspects and implementation.

CONCLUSIONS

Our method is related directly to MVA and is valid for any 2-D velocity fields. We have shown how to use information from locally coherent events picked in the migrated cube. These events are treated independently up front, i.e., not attached to a specific reflector. If extra information such as correlations between these events is introduced, the inversion should be better constrained. Our method provides a smooth velocity model consistent with Kirchhoff-type migration schemes, but the theory could be developed equivalently for blocky models. The method could be called tomographic migration velocity analysis or stereotomography in depth because it links two different velocity estimation methods working in different space, time, and depth domains.

We know that the occurrence of coherent noise such as multiples or refracted waves remains a problem because it could bias the velocity inversion, but this aspect is not specific to our method. The details of the practical aspects are developed in Chauris et al. (2002) that also includes applications to 2-D synthetic and real data sets, showing the efficiency of the method.

ACKNOWLEDGMENTS

This work was partially funded by the European Commission within the JOULE project, 3D-Focus (contract JOF3-CT97-0029).

REFERENCES

Adler, F., 1996, Tomographie de réflexion à partir des images migrées avant addition: Ph.D. thesis, Université de Pau et des Pays de l'Adour.

Aki, K., and Richards, P. G., 1980, Quantitative Seismology: Theory and Methods: W. H. Freeman & Co.

Al-Yahya, K., 1989, Velocity analysis by iterative profile migration: Geophysics, **54**, 718–729.

Audebert, F., Diet, J. P., Guillaume, P., Jones, I., and Zhang, X., 1997, CRP Scan: 3-D preSDM velocity analysis via zero offset tomographic inversion: 67th Ann. Internat. Mtg., Soc. Expl. Geophys., Expanded Abstracts, 1805–1808.

Billette, F., and Lambaré, G., 1998, Velocity macro-model estimation from seismic reflection data by stereotomography: Geophys. J. Internat., **135**, 671–680.

Billette, F., Podvin, P., and Lambaré, G., 1998, Stereotomography with automatic picking: Application to the Marmousi dataset: 68th Ann. Internat. Mtg., Soc. Expl. Geophys., Expanded Abstracts, 1317–1320.

Biondi, B., 1992, Velocity estimation by beam stack: Geophysics, **57**, 1034–1047.

Bleistein, N., Cohen, J., and Hagin, F., 1987, Two-and-one-half dimensional Born inversion with an arbitrary reference: Geophysics, **52**, 26–36.

Burridge, R., 1976, Some mathematical topics in seismology: Courant Inst. of Math. Sciences.
Červený, V., Molotkov, I. A., and Psencik, I., 1997, Ray theory in seismology: Charles Univ. Press.
Chauris, H., and Noble, M., 1998, Differential semblance optimization for 2D velocity field estimation: Soc. Expl. Geophys./Eur. Assn. Geosci. Eng., Extended Abstracts for Workshop on Depth Imaging of Reservoir Attributes X012.
——— 2001, Two-dimensional velocity model estimation from seismic reflection data by local differential semblance optimization: Application to synthetic and real data sets: Geophys. J. Internat., **144**, 14–26.
Chauris, H., Noble, M. S., Lambaré, G., and Podvin, P., 2002, Migration velocity analysis from locally coherent events in 2-D laterally heterogeneous media, Part II: Applications on synthetic and real data: Geophysics, **67**, 1213–1224.
Clément, F., 1994, Une formulation en temps de parcours par migration pour la détermination des vitesses de propagation acoustique à partir de données sismiques bidimensionnelles: Ph.D. thesis, Université Paris IX Dauphine.
Cox, H. L. H., and Wapenaar, C. P. A., 1992, Macro model estimation by common offset migration and by shot record migration: J. Seismic Expl., **1**, 29–37.
Deregowski, S. M., 1990, Common-offset migrations and velocity analysis: First Break, **8**, 225–234.
Docherty, P., Silva, R., Singh, S., Song, Z., and Wood, M., 1997, Migration velocity analysis using a genetic algorithm: Geophys. Prosp., **45**, 865–878.
Farra, V., and Madariaga, R., 1987, Seismic waveform modeling in heterogeneous media by ray perturbation theory: J. Geophys. Res., **92**, 2697–2712.
Jervis, M., Sen, M., and Stoffa, P., 1996, Prestack migration velocity estimation using nonlinear methods: Geophysics, **61**, 138–150.
Jin, S., and Beydoun, W., 2000, 2D multiscale non-linear velocity estimation: Geophys. Prosp., **48**, 163–180.
Jin, S., and Madariaga, R., 1993, Background velocity inversion with a genetic algorithm: Geophys. Res. Lett., **20**, No. 2, 93–96.
——— 1994, Nonlinear velocity inversion by a two-step Monte Carlo: Geophysics, **59**, 577–590.
Lafond, C. F., and Levander, A. R., 1993, Migration moveout analysis and depth focusing: Geophysics, **58**, 582–598.
Lambaré, G., Lucio, P. S., and Hanyga, A., 1996, Two-dimensional multivalued traveltime and amplitude maps by uniform sampling of ray field: Geophys. J. Internat., **125**, 584–598.
Lee, W., and Zhang, L., 1992, Residual shot profile migration: Geophysics, **57**, 815–822.
Liu, Z., 1997, An analytical approach to migration velocity analysis: Geophysics, **62**, 1238–1249.
Liu, Z., and Bleistein, N., 1995, Migration velocity analysis: Theory and an iterative algorithm: Geophysics, **60**, 142–153.
Nolan, C., and Symes, W., 1996, Imaging in complex velocities with general acquisition geometry: The Rice Inversion Project Technical Report TR96-02.
Plessix, R. E., 1996, Détermination de la vitesse pour l'interprétation de données sismiques très haute résolution à l'échelle géotechnique: Ph.D. thesis, Université Paris IX Dauphine.
Schneider, W. A., 1978, Integral formulation for migration in two and three dimensions: Geophysics, **43**, 49–76.
Schultz, P. S., and Claerbout, J. F., 1978, Velocity estimation and downward continuation by wavefront synthesis: Geophysics, **43**, 691–714.
Stoffa, P. L., 1989, Tau-p: A plane wave approach to the analysis of seismic data: Kluwer Academic Publishers.
Sword, C. H., 1987, Tomographic determination of interval velocities from reflection seismic data: The method of controlled directional reception: Ph.D. thesis, Stanford University.
Stork, C. H., 1992, Reflection tomography in the postmigrated domain: Geophysics, **57**, 680–692.
Symes, W. W., 1993, A differential semblance criterion for inversion of multioffset seismic reflection data: J. Geophys. Res., **98**, 2061–2073.
——— 1998, High frequency asymptotics, differential semblance, and velocity estimation: 68th Ann. Internat. Mtg., Soc. Expl. Geophys., Expanded Abstracts, 1616–1619.
——— 1999, All stationary points of differential semblance are asymtotic global minimizers: Layered acoustics: The Rice Inversion Project Technical Report TR99-09.
Symes, W. W., and Carazzone, J., 1991, Velocity inversion by differential semblance optimization: Geophysics, **56**, 654–663.
ten Kroode, A. P. E., and Smit, D. J., 1997, A microlocal analysis of a linearized inversion problem: SIAM Inverse Problems in Geophysical Applications, 146–162.
Tygel, M., Schleicher, J., and Hubral, P., 1994, Pulse distortion in depth migration: Geophysics, **59**, 1561–1569.
Varela, C. L., Stoffa, P. L., and Sen, M. K., 1998, Background velocity estimation using non-linear optimization for reflection tomography and migration misfit: Geophys. Prosp., **46**, 51–78.
Virieux, J., 1996, Seismic ray tracing, *in* Boschi, E., Ekstrom, G., and Morelli, A., Eds., Seismic modelling of earth structure: Istituto Nazionale di Geofisica, 223–300.
Wang, B., Pann, K., and Meek, R. A., 1995, Macro velocity model estimation through model-based globally-optimized residual-curvature analysis: 65th Ann. Internat. Mtg., Soc. Expl. Geophys., Expanded Abstracts, 1084–1087.
Woodward, M., Farmer, P., Nichols, D., and Charles, S., 1998, Automated 3D tomographic velocity analysis of residual moveout in prestack migrated common image point gathers: 68th Ann. Internat. Mtg., Soc. Expl. Geophys., Expanded Abstracts, 1218–1221.
Xu, S., Chauris, H., Lambaré, G., and Noble, M., 2001, Common angle migration: A strategy for imaging complex media: Geophysics, **66**, 1877–1894.

APPENDIX A

COST FUNCTION

We explain how to derive equation (18) from equation (17) to express the residual slope with local quantities. As illustrated (Figure A-1), we have

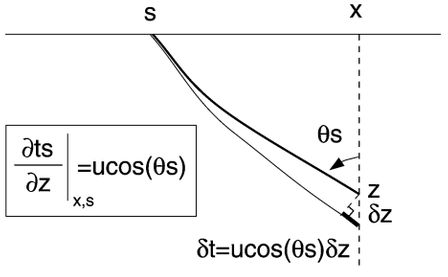

FIG. A-1. For a given source position and a velocity model, the derivative of the traveltime from the source to the scattering point with respect of the final depth depends on the arrival angle and the value of the slowness field.

$$\left.\frac{\partial t_s}{\partial z}\right|_{s,x,u} = u(x,z)\cos\theta_s, \tag{A-1}$$

$$\left.\frac{\partial t_r}{\partial z}\right|_{x,r,u} = u(x,z)\cos\theta_r, \tag{A-2}$$

where $u(x,z)$ is the slowness value at the scattering point. Using

$$\cos\theta_s + \cos\theta_r = 2\cos\theta\cos\xi, \tag{A-3}$$

we obtain

$$\left.\frac{\partial t_s}{\partial z}\right|_{s,x,u} + \left.\frac{\partial t_r}{\partial z}\right|_{r,x,u} = 2u(x,z)\cos\theta\cos\xi = \alpha, \tag{A-4}$$

which is needed for the equivalent equations (18) and (20).

APPENDIX B
GRADIENT COMPUTATION

We now compute the gradient of the cost function using the paraxial ray theory, first for the common-shot case and then for the common-offset case. As expressed in equation (38), the gradient of the cost function in common-shot migration is given by

$$\frac{\partial J[u]}{\partial u} = 2\sum_{picks} u\cos\theta\cos\xi\tan\varphi\left.\frac{\partial p_{sx}}{\partial u}\right|_{s,r,t,p_{rx}}, \quad \text{(B-1)}$$

The perturbations $\delta s, \delta r, \delta p_{sx}$, and δp_{rx} of the final conditions on surface are linked through the paraxial ray theory to the initial perturbations δz, $\delta\theta_s$, and $\delta\theta_r$ at the scattering point and to the slowness field δu. They can be expressed along the rays using the propagator matrix (Aki and Richards, 1980) as follows:

$$\begin{pmatrix}\delta s\\ \delta s_z\\ \delta p_{sx}\\ \delta p_{sz}\end{pmatrix} = P_s(\tau,\tau_0)\begin{pmatrix}\delta x\\ \delta z\\ \delta p_{sx0}\\ \delta p_{sz0}\end{pmatrix} + P_s(\tau,\tau_0) \times \int_{\tau_0}^{\tau} d\tau' P_s^{-1}(\tau',\tau_0)\begin{pmatrix}0\\ \nabla u\delta u\end{pmatrix}, \quad \text{(B-2)}$$

$$\begin{pmatrix}\delta r\\ \delta r_z\\ \delta p_{rx}\\ \delta p_{rz}\end{pmatrix} = P_r(\tau,\tau_0)\begin{pmatrix}\delta x\\ \delta z\\ \delta p_{rx0}\\ \delta p_{rz0}\end{pmatrix} + P_r(\tau,\tau_0) \times \int_{\tau_0}^{\tau} d\tau' P_r^{-1}(\tau',\tau_0)\begin{pmatrix}0\\ \nabla u\delta u\end{pmatrix}, \quad \text{(B-3)}$$

where δs_z and δr_z should equal zero as the ray segments end at the surface. The perturbation $\delta\theta_s$ is linked to the perturbations of the slowness vectors δp_{sx0} and δp_{sz0} at the scattering point by $p_{sx0} = u\sin\theta_s$ and $p_{sz0} = u\cos\theta_s$. In practice, we used a second-order Runge–Kutta method to integrate the rays and the perturbations. The parameter along the ray is τ (Burridge, 1976; Virieux, 1996), given by $d\tau = vd\sigma$ (where σ is the curvilinear abscissa). The propagator is a 2×2 matrix, determined by (Farra and Madariaga, 1987)

$$\frac{\partial P}{\partial\tau} = \begin{pmatrix}0 & I\\ \frac{1}{2}\nabla\nabla u^2 & 0\end{pmatrix}P, \quad \text{(B-4)}$$

$$P(\tau_0,\tau_0) = I, \quad \text{(B-5)}$$

where I is the 2×2 identity matrix. The four focusing conditions state that the source s and receiver r positions, the total traveltime t, and the slope at the receiver p_{rx} are constant. They all depend on x, z, $\delta\theta_s$, $\delta\theta_r$, and u. Remember that the differentiation of a variable can be expressed as follows:

$$d\cdot = \left.\frac{\partial\cdot}{\partial x}\right|_{u,z,\theta_s,\theta_r}\delta x + \left.\frac{\partial\cdot}{\partial z}\right|_{u,x,\theta_s,\theta_r}\delta z + \left.\frac{\partial\cdot}{\partial\theta_s}\right|_{u,x,z,\theta_r}\delta\theta_s + \left.\frac{\partial\cdot}{\partial\theta_r}\right|_{u,x,z,\theta_s}\delta\theta_r + \left.\frac{\partial\cdot}{\partial u}\right|_{x,z,\theta_s,\theta_r}\delta u. \quad \text{(B-6)}$$

The gradient of the cost function needs to differentiate the slope at the source position and finally express it as a function of δu. Conditions $[ds=0; dr=0; dt=0; dp_{rx}=0; dp_{sx}=K\delta u]$ can be expressed as

$$\begin{pmatrix}dp_{sx}\\ ds\\ dr\\ dt\\ dp_{rx}\end{pmatrix} = \begin{pmatrix}dp_{sx}\\ 0\\ 0\\ 0\\ 0\end{pmatrix} = \left(\frac{\partial(p_{sx},s,r,t,p_{rx})}{\partial(u,x,z,\theta_s,\theta_r)}\right)\cdot\begin{pmatrix}\delta u\\ \delta x\\ \delta z\\ \delta\theta_s\\ \delta\theta_r\end{pmatrix}. \quad \text{(B-7)}$$

Solving the linear system given by equation (B-7), we obtain the final formula (39).

The common-offset case is very similar to the previous case; p_{hx} and p_{mx} are defined in equations (21) and (22). The equations $dh=0$, $dm=0$, $dt=0$, and $dp_{mx}=0$ define a system of four linear equations which let us determine $\delta x, \delta z, \delta\xi$, and $\delta\theta$. We thus solve

$$\begin{pmatrix}dp_{hx}\\ dh\\ dm\\ dt\\ dp_{mx}\end{pmatrix} = \begin{pmatrix}dp_{hx}\\ 0\\ 0\\ 0\\ 0\end{pmatrix} = \left(\frac{\partial(p_{hx},h,m,t,p_{mx})}{\partial(u,x,z,\xi,\theta)}\right)\cdot\begin{pmatrix}\delta u\\ \delta x\\ \delta z\\ \delta\xi\\ \delta\theta\end{pmatrix} \quad \text{(B-8)}$$

to obtain the final formula (41).